Communication

A Compact and Wideband Linear Array Antenna With Low Mutual Coupling

Seongjung Kim and Sangwook Nam

***Abstract*— A low mutual coupling array antenna operating in the *Ku*-band is proposed. To reduce mutual coupling, side metallic walls with a small resistive film are incorporated into both sides of the dipole antenna. These walls can also help impedance matching across the whole *Ku*-band. By investigating the current density distribution on the side wall with frequency, the appropriate positions of the resistive films are determined. Finally, the design is tested by measurement, which is in good agreement with simulation results. The performance is as follows: the operating bandwidth (OBW) is 11.9–20.3 GHz (52.2%) for the impedance bandwidth (IBW) with −10 dB and the low mutual coupling band with less than −20 dB. The radiation efficiency is over 63.9%. The active element gain is 1.88–4.57 dBi. The measured array gain is 15–16.7 dBi as scanning the beam from 0° to 45° at 16 GHz. The OBW is almost constant up to scan angle of 45°. The overall dimensions of the array structure with 17 elements are 1.2 × 9.2 × 0.44λ_{low} at the lowest operating frequency of 12 GHz.**

***Index Terms*— Beamforming array antenna, compact array, compact low mutual coupling array, multi-input multi-output (MIMO) antenna, wideband low mutual coupling array.**

I. Introduction

As demands for higher data rates have been increasing, the wideband beamforming array antenna is expanding [1]. To obtain the optimal performance of the beamforming array antenna, several factors should be considered. One factor is the mutual coupling that distorts the signal fed to each antenna element, which affects the pattern of array antennas [2], [3]. In addition, mutual coupling affects the impedance matching characteristics [4]. The mutual coupling can be reduced by placing the antenna elements far apart. However, to avoid the appearance of grating lobes, the distances between antennas should not be too great.

There are several ways to reduce mutual coupling between adjacent antenna elements. For microstrip antennas, one can insert a metal fence between the antenna elements [5]. This can block the surface wave along the substrate. In some cases, currents flowing along the ground plane can generate mutual coupling between antenna elements. This can be suppressed by utilizing defected ground structures to block the currents [6]–[10]. Another strategy is to connect the neutralization line directly between adjacent antenna elements [11], [12]. This line decouples two antennas at the resonance frequency band. A decoupling network can also be designed below the antenna to reduce mutual coupling [13], [14]. Recently, a metamaterial-inspired structure or an electromagnetic bandgap (EBG) structure was utilized between antenna elements as an isolator [15]–[17]. However, there is a drawback when applying these techniques to broadband beamforming array antenna systems: they all [5]–[17] operate only in a narrow band, except for [12]. Although many studies address the reduction of mutual coupling in multi-input-multi-output (MIMO) antennas at LTE, Bluetooth, WLAN, and ISM bands, only a few studies effort to reduce the mutual coupling of phased array antennas [5], [15] or MIMO antennas for applications above the X-band [18]–[20].

Manuscript received January 29, 2019; revised April 23, 2019; accepted May 29, 2019. Date of publication June 19, 2019; date of current version August 12, 2019. This work was supported in part by the NATO Science for Peace and Security Programme under Grant G5395 and in part by the Brain Korea 21 Plus Project in 2018. *(Corresponding author: Seongjung Kim.)*

The authors are with the School of Electrical and Computer Engineering, Institute of New Media Communication (INMC), Seoul National University, Seoul 08826, South Korea (e-mail: sjkim@ael.snu.ac.kr).

Color versions of one or more of the figures in this communication are available online at http://ieeexplore.ieee.org.

Digital Object Identifier 10.1109/TAP.2019.2922833

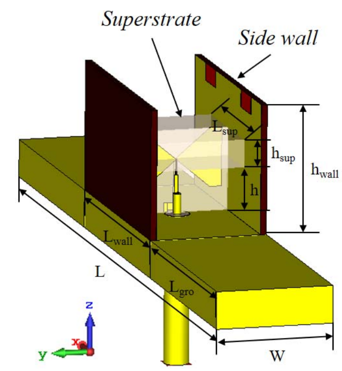

Fig. 1. Configuration of proposed unit cell antenna (L = 60 mm, L_{gro} = 20 mm, L_{wall} = 20 mm, L_{sup} = 10 mm, W = 10 mm, h = 4.64 mm, h_{sup} = 2.36 mm, h_{wall} = 11 mm).

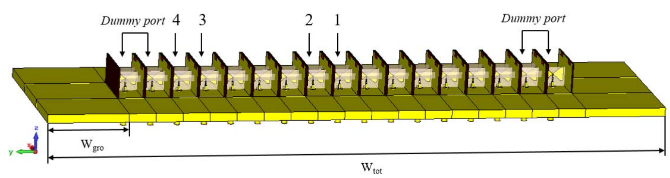

Fig. 2. Dimensions of the full array structure (17 elements) are 30 × 230 × 11 mm (W_{gro} = 30 mm and W_{tot} = 230 mm).

In this communication, a new approach is described to reduce mutual coupling between the array elements in a 1-D array for wideband applications. This can be achieved by electric side walls and resistive films. In Section II, the effects of electric side walls on impedance matching and mutual coupling are described. The method for determining the position where the resistive films are laminated and the size of films for efficiently reducing the mutual coupling are also described. In Section III, the method is verified by measurement. Finally, the work is concluded in Section IV.

II. Design of Antenna Structure and Operation

The configuration of the proposed unit cell antenna is shown in Fig. 1. This antenna is fed by a single-ended coaxial cable. Superstrates are used to obtain wideband characteristics. The superstrate has a thickness of h_{sup} and is composed of Taconic TLY-5 (ε_r = 2.2, $tan\delta$ = 0.0009). The full array configuration is shown in Fig. 2. The number of elements is 17, and the extra four elements at either end are dummy elements for a consistent radiation pattern.

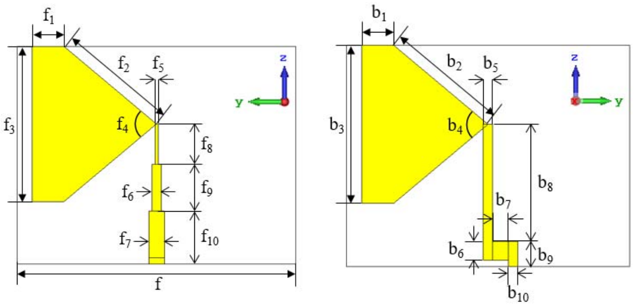

(a) **(b)**

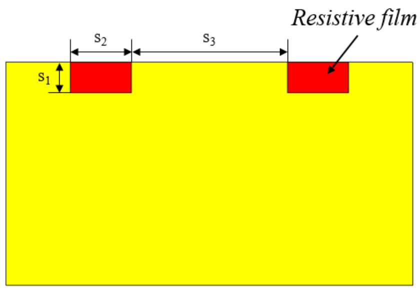

(c)

Fig. 3. Dimension of (a) PCB of front side, (b) back side, and (c) side wall laminated with resistive films ($f = 8.96$ mm, $f_1 = 1.02$ mm, $f_2 = 3.89$ mm, $f_3 = 5$ mm, $f_4 = 80°$, $f_5 = 0.1$ mm, $f_6 = 0.3$ mm, $f_7 = 0.5$ mm, $f_8 = 1.3$ mm, $f_9 = 1.5$ mm, $f_{10} = 1.7$ mm, $b_1 = 1.02$ mm, $b_2 = 3.89$ mm, $b_3 = 5$ mm, $b_4 = 80°$, $b_5 = 0.3$ mm, $b_6 = 0.6$ mm, $b_7 = 0.5$ mm, $b_8 = 3.7$ mm, $b_9 = 0.8$ mm, $b_{10} = 0.3$ mm, $s_1 = 1.5$ mm, $s_2 = 3$ mm, and $s_3 = 7.67$ mm).

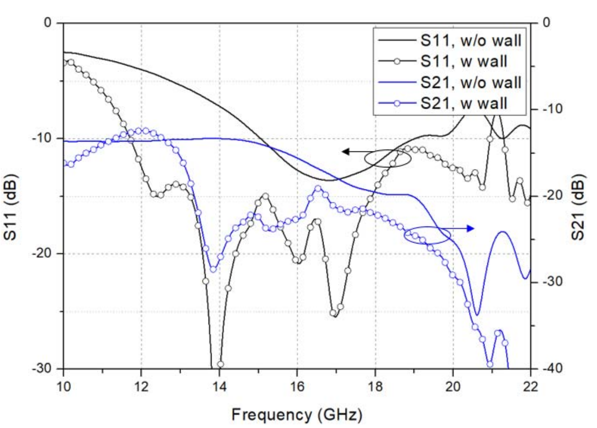

Fig. 4. Effect of electric side walls without resistive films on the dipole antenna characteristic.

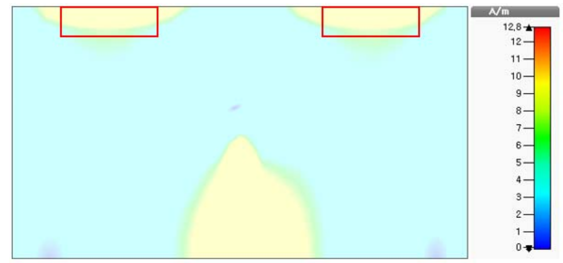

Fig. 5. Distribution of current density on the side wall before laminating resistive films on the wall at 12 GHz.

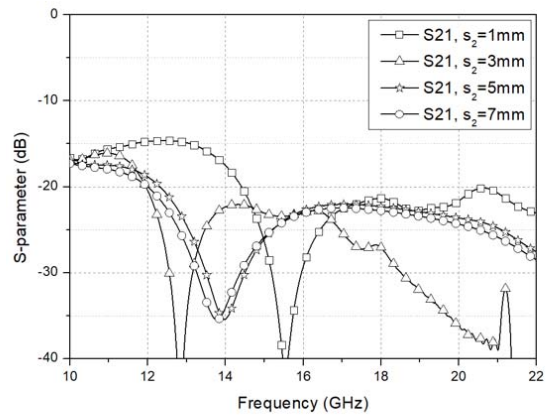

(a)

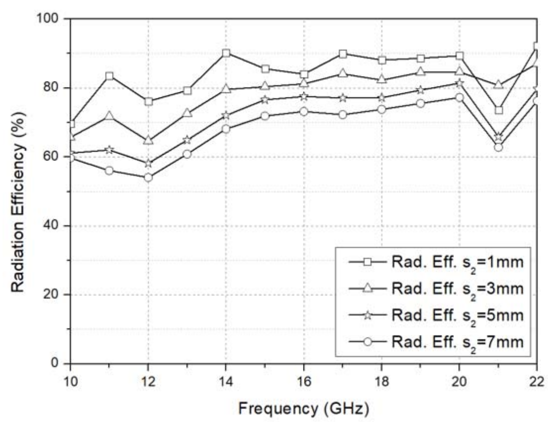

(b)

Fig. 6. Parametric studies on the effect of the length of resistive films ($s_1 = 1.5$ mm) on (a) mutual coupling and (b) radiation efficiency.

The edge elements are numbered 1 to 4. The dimensions of the side wall and the printed circuit board (PCB) of the dipole antenna are shown in Fig. 3. The dielectric material of the PCB is TLY-5 with a thickness of 0.25 mm. The feeding line is composed of a stepped impedance line on the front side of the PCB. The resistive thin film has a resistance of 377 Ω/□ (https://ohmega.com) and it is laminated on FR-4 ($\varepsilon_r = 4.3, tan\delta = 0.025$) with a thickness of 0.5 mm.

The side wall plays two roles. First, it helps the dipole antenna to operate over wideband. Second, it reduces the mutual coupling between dipole antennas, as shown in Fig. 4. However, the side wall cannot suppress mutual coupling at the low-frequency band because the interelement spacing is small, and there is strong diffraction via the edge of the side wall. In fact, the size of the side wall does not need to keep increasing to lower the mutual coupling.

Fig. 5 shows the electric current density on the side wall indicated in Fig. 3(c) without laminating resistive films on the wall at 12 GHz. Without resistive films, the current strongly flows on the edge of the side wall denoted as a red line box at 12 GHz. As a result, resistive films are laminated on the position to dissipate the power carried by the current flowing there and reduce the mutual coupling efficiently. Note that the resistive films have little effect on the original distribution of current density on the side wall because the size of the film is very small, i.e., only $0.12 \times 0.06\lambda_{\text{low}}$ at 12 GHz.

Fig. 6 shows parametric studies on the effect of the length of resistive films. When the length of the film is 3 mm, the mutual

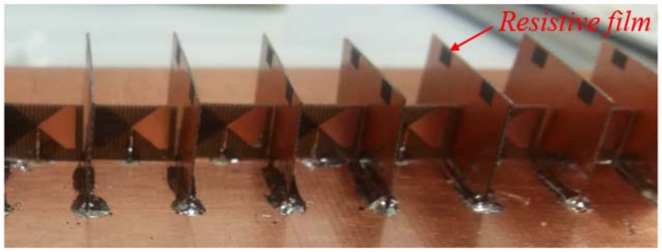

(a)

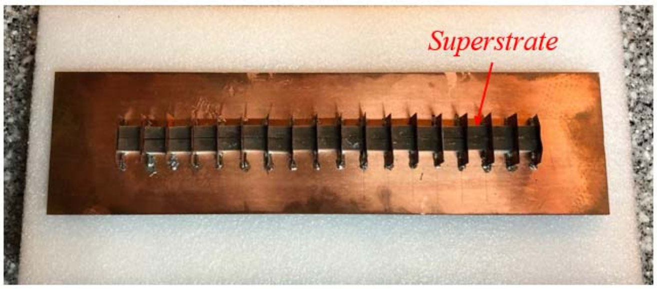

(b)

Fig. 7. Prototype of the full array structure (a) without (side view) and (b) with superstrates (top view).

coupling is greatly reduced at the low-frequency band. However, if the length exceeds 3 mm, the effect on reducing coupling is small, while the radiation efficiency is progressively degraded.

III. Simulated and Measured Results for the Proposed Antenna

A. Active Element Gain and Radiation Efficiency

The prototype of the 17-element full array antenna is shown in Fig. 7. The dimensions are $30 \times 230 \times 11$ mm. The black rectangles shown in Fig. 7(a) are the resistive films. The superstrates are supported by the Rohacell material whose relative permittivity is nearly one (https://www.rohacell.com). The gain pattern and radiation efficiency were measured in an anechoic chamber (https://iot.nipa.kr). They can support measurements of up to 18 GHz for a 3-D beam pattern, which is relevant when measuring radiation efficiency. The measurement of the S-parameter was implemented by a PNA network analyzer from Agilent Technologies. All the simulations were performed by the computer simulation technology (CST) electromagnetic (EM) tool. To verify the uniformity of the characteristics of different elements, only the results of two ports (1 and 4) in Fig. 2 are shown.

In Fig. 8, the simulated and measured overlapped impedance bandwidth (IBW) for −10 dB is 11.2–21.1 GHz and 10.9–20.3 GHz, respectively. The simulated and measured mutual couplings are both below −20 dB over 11.9 GHz. Fig. 9 shows that the simulated and measured radiation efficiency for ports 1 and 4 is over 65.0% and 63.9%, respectively, within the operating bandwidth (OBW) (11.9–20.3 GHz). As expected, the degradation of radiation efficiency at 12 GHz is largest because the positioning of the resistive films is aimed at the low-frequency band. In fact, data regarding the measured radiation efficiency at 18 GHz is absent because the measurement of the 3-D gain pattern could not be supported. Fig. 10 shows the active element gain. The simulated and measured gain is 2.04–4.15 dBi and 1.88–4.57 dBi, respectively, within the OBW. In addition, the measured Xpol/Copol is below −15 dB and the back/broadside level is below −25 dB within the OBW. Fig. 11 shows the normalized gain

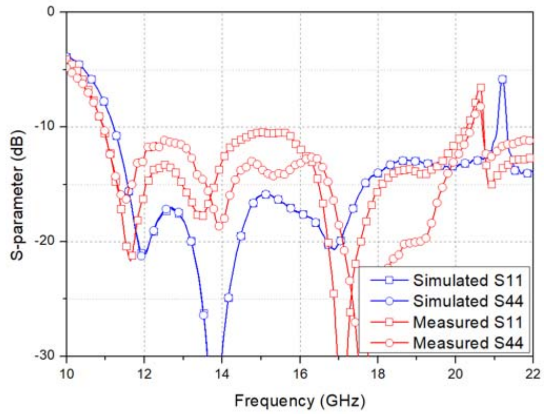

(a)

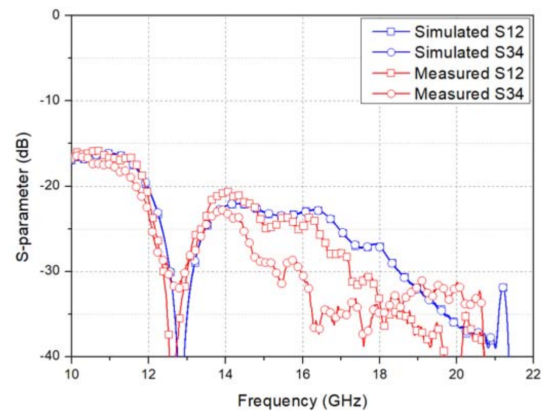

(b)

Fig. 8. Simulated and measured results of (a) impedance matching property and (b) mutual coupling characteristic.

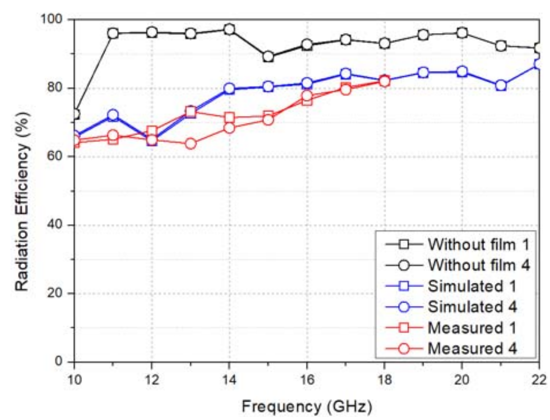

Fig. 9. Simulated and measured radiation efficiency.

pattern at 12, 16, and 20 GHz. The measured overall pattern is in good agreement with the simulated pattern.

B. Array Performances

In this section, the proposed array antenna is fully excited (except for dummy ports) and the array performances are shown. Fig. 12 shows the simulated active reflection coefficient. Without the side walls, the impedance matching is quite poor when scanning the beam from 0° to 45°. By contrast, the impedance matching of the proposed antenna is good up to 45°, which is due to the reduced

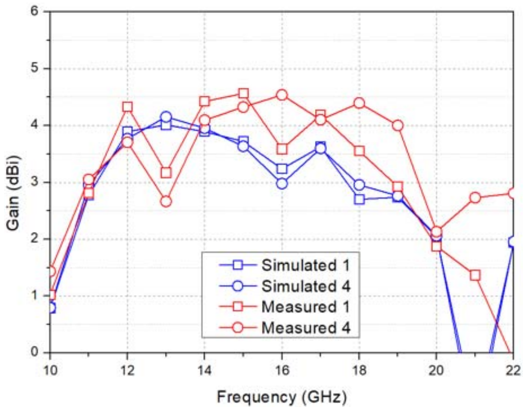

Fig. 10. Simulated and measured active element gain.

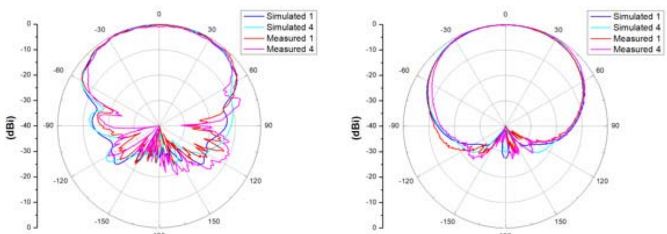

(a)

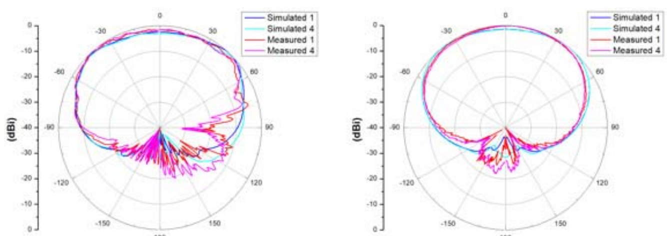

(b)

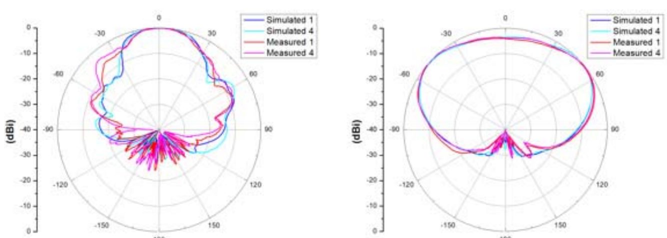

(c)

Fig. 11. Simulated and measured normalized active element gain pattern on *yz* plane (left column) and *xz* plane (right column) at (a) 12 GHz, (b) 16 GHz, and (c) 20 GHz.

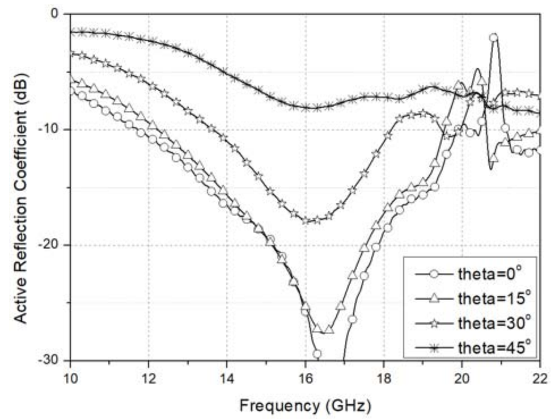

(a)

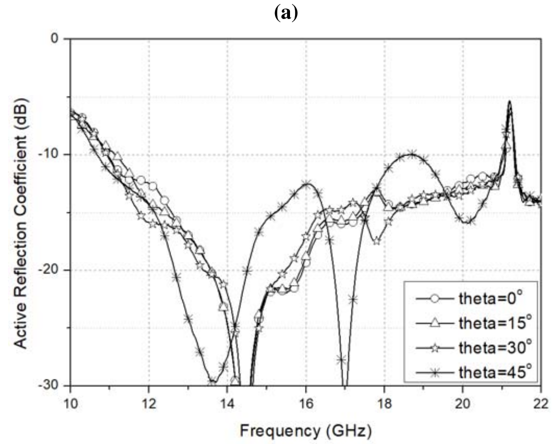

(b)

Fig. 12. Simulated active reflection coefficient as beam scanning from 0° to 45° (a) without and (b) with side walls.

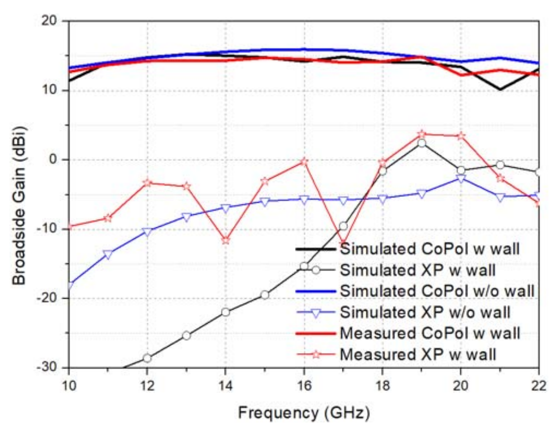

Fig. 13. Simulated and measured broadside array gain.

mutual coupling of the proposed antenna. Therefore, the bandwidth of fully and not fully excited array antennas is almost the same, which can be seen when comparing Figs. 8(a) and 12(b). The array gain is measured based on [21]. This method is based on the following equation:

$$E(\theta,\phi) = \sum_{i=1}^{N} V_i g_i(\theta,\phi) \tag{1}$$

where N is the total number of elements (it is 13 in this case), V_i is the complex value of the excitation, i is the number of ports, and $g_i(\theta, \varphi)$ is the active element gain pattern of the ith element. When $g_i(\theta, \varphi)$ is measured, the other elements are matched and terminated. The measured results are in good agreement with the simulated results, as shown in Figs. 13 and 14. In Fig. 13, the simulated and measured broadside gain of the proposed array antenna is around 15 dBi within the OBW. The measured cross polarization level is less than −8.9 dB. The simulated broadside array gain, without side walls, is around 15.9 dBi, and the simulated cross polarization is less than −16.7 dB. By introducing the side walls, the broadside gain is slightly degraded, which is partially due to the reduction in radiation efficiency. The radiation gain pattern on the *yz* plane and the *xz* plane at 16 GHz is shown in Fig. 14. The measured sidelobe level of the proposed array antenna is lower than −9.8 dB. On the *xz* plane, by introducing the side walls, the broadside gain is slightly degraded; however, the difference is less than 1 dB.

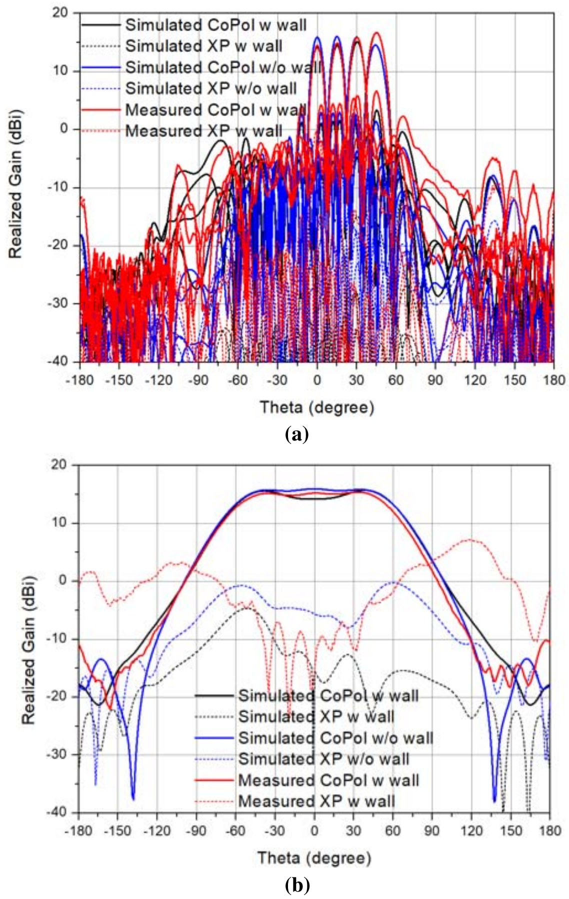

Fig. 14. Simulated and measured results of realized gain as beam scanning from 0° to 45° on (a) *yz* plane and (b) *xz* plane at 16 GHz.

IV. Conclusion

In this communication, we proposed a wideband and low mutual coupling array antenna using a conducting side wall with resistive films. The side wall can make the IBW of dipole antennas wider and the mutual coupling lower. Additionally, the mutual coupling at low frequencies can be reduced by resistive films on the side wall. Investigating the parametric studies on the length of resistive films, the appropriate size of films was chosen to selectively reduce mutual coupling without a severe reduction in radiation efficiency at other frequency bands. Moreover, it was shown that the side wall improves the impedance matching property as scanning the beam by reducing the mutual coupling. Finally, it is expected that this array antenna could be used in radar systems or MIMO communication systems.

References

[1] T. Do-Hong and P. Russer, "Signal processing for wideband smart antenna array applications," *IEEE Microw. Mag.*, vol. 5, no. 1, pp. 57–67, Mar. 2004.

[2] A. M. Wyglinski and S. D. Blostein, "On uplink CDMA cell capacity: Mutual coupling and scattering effects on beamforming," *IEEE Trans. Veh. Technol.*, vol. 52, no. 2, pp. 289–304, Mar. 2003.

[3] C. M. Schmid, S. Schuster, R. Feger, and A. Stelzer, "On the effects of calibration errors and mutual coupling on the beam pattern of an antenna array," *IEEE Trans. Antennas Propag.*, vol. 61, no. 8, pp. 4063–4072, Apr. 2013.

[4] A. K. Bhattacharyya, *Phased Array Antennas: Floquet Analysis, Synthesis, BFNs and Active Array Systems*, vol. 179. Hoboken, NJ, USA: Wiley, 2006.

[5] B. A. Arand, A. Bazrkar, and A. Zahedi, "Design of a phased array in triangular grid with an efficient matching network and reduced mutual coupling for wide-angle scanning," *IEEE Trans. Antennas Propag.*, vol. 65, no. 6, pp. 2983–2991, Jun. 2017.

[6] C.-Y. Chiu, C.-H. Cheng, R. D. Murch, and C. R. Rowell, "Reduction of mutual coupling between closely-packed antenna elements," *IEEE Trans. Antennas Propag.*, vol. 55, no. 6, pp. 1732–1738, Jun. 2007.

[7] S. Xiao, M.-C. Tang, Y.-Y. Bai, S. Gao, and B.-Z. Wang, "Mutual coupling suppression in microstrip array using defected ground structure," *IET Microw., Antennas Propag.*, vol. 5, no. 12, pp. 1488–1494, Sep. 2011.

[8] K. Wei, J.-Y. Li, L. Wang, Z.-J. Xing, and R. Xu, "Mutual coupling reduction by novel fractal defected ground structure bandgap filter," *IEEE Trans. Antennas Propag.*, vol. 64, no. 10, pp. 4328–4335, Oct. 2016.

[9] D. Wu, S. W. Cheung, Q. L. Li, and T. I. Yuk, "Decoupling using diamond-shaped patterned ground resonator for small MIMO antennas," *IET Microw., Antennas Propag.*, vol. 11, no. 2, pp. 177–183, Jan. 2017.

[10] S. J. Yoon and J. Choi, "A low-profile broadband array antenna for home repeater applications," *J. Electromagn. Eng. Sci.*, vol. 18, no. 4, pp. 261–266, Oct. 2018.

[11] S.-W. Su, C.-T. Lee, and F.-S. Chang, "Printed MIMO-antenna system using neutralization-line technique for wireless USB-dongle applications," *IEEE Trans. Antennas Propag.*, vol. 60, no. 2, pp. 456–463, Feb. 2012.

[12] S. Zhang and G. F. Pedersen, "Mutual coupling reduction for UWB MIMO antennas with a wideband neutralization line," *IEEE Antennas Wireless Propag. Lett.*, vol. 15, pp. 166–169, 2016.

[13] S.-C. Chen, Y.-S. Wang, and S.-J. Chun, "A decoupling technique for increasing the port isolation between two strongly coupled antennas," *IEEE Trans. Antennas Propag.*, vol. 56, no. 12, pp. 3650–3658, Dec. 2008.

[14] L. Zhao, L. K. Yeung, and K.-L. Wu, "A coupled resonator decoupling network for two-element compact antenna arrays in mobile terminals," *IEEE Trans. Antennas Propag.*, vol. 62, no. 5, pp. 2767–2776, May 2014.

[15] S. Hwang, B. Lee, D. H. Kim, and J. Y. Park, "Design of S-band phased array antenna with high isolation using broadside coupled split ring resonator," *J. Electromagn. Eng. Sci.*, vol. 18, no. 2, pp. 108–116, Apr. 2018.

[16] R. Hafezifard, M. Naser-Moghadasi, J. R. Mohassel, and R. A. Sadeghzadeh, "Mutual coupling reduction for two closely spaced meander line antennas using metamaterial substrate," *IEEE Antennas Wireless Propag. Lett.*, vol. 15, pp. 40–43, 2016.

[17] S. Ebadi and A. Semnani, "Mutual coupling reduction in waveguide-slot-array antennas using electromagnetic bandgap (EBG) structures," *IEEE Antennas Propag. Mag.*, vol. 56, no. 3, pp. 68–79, Jun. 2014.

[18] Nirdosh, S. Sah, and A. Kakkar, "Ament wideband MIMO antenna for X-band, Ku-band, K-band applications," in *Proc. 5th Int. Conf. Signal Process. Integr. Netw. (SPIN)*, Feb. 2018, pp. 94–97.

[19] Nirdosh, C. M. Tan, and M. R. Tripathy, "A miniaturized T-shaped MIMO antenna for X-band and Ku-band applications with enhanced radiation efficiency," in *Proc. 27th Wireless Opt. Commun. Conf. (WOCC)*, Apr. 2018, pp. 1–5.

[20] H. U. Habiba, A. Narasimhan, A. R. Narayanan, S. Revathy, S. Priya, and A. E. Ramanujan, "Compact half-ellipse co-radiator MIMO antenna," in *Proc. Int. Conf. Wireless Commun., Signal Process. Netw. (WiSPNET)*, Mar. 2016, pp. 1022–1025.

[21] D. F. Kelley and W. L. Stutzman, "Array antenna pattern modeling methods that include mutual coupling effects," *IEEE Trans. Antennas Propag.*, vol. 41, no. 12, pp. 1625–1632, Dec. 1993.